Rotorcraft MAV having and Onboard manipulator : Longitudinal Modeling and Robust Control.

Juan Antonio Escareño, Micky Rakotondrabe, Gerardo Ramon Flores, Rogelio Lozano

Rotorcraft MAV Having an Onboard Manipulator: Longitudinal Modeling and Robust Control

J. Escareno, M. Rakotondrabe, G. Flores and R. Lozano

Abstract— The paper presents results on the modeling and control of a multi-body air vehicle concept that incorporates a robotic arm to a miniatute rotorcraft robot. One of our goals was to obtain a detailed model in order to identify and qualify inherent constraints provided by the interaction of both mechanical subsystems.To do this, we used the Euler-Lagrange formulation. The knowledge of the model of the interactive aerial robot allowed us to propose a hierarchical control scheme, where a nonlinear Sliding Mode Controller (SMC) handle the translational motion while the rotational motion is addressed by a H_∞-based controller. Numerical simulations were carried out to validate the overal control approach.

I. Introduction

The applications of Miniature Air Vehicles (MAVs) have widely diversified during the last years. They comprise both military and civilian, though the latter has had a lower development rate. The main goal of Unmanned Air Vehicles (UAVs) is to provide a remote and mobile extension of human perceptions, allowing not only the security of the user (soldier, policeman, cameraman, volcanologist) but also the collection of valuable information of zones/targets of interest used for online or offline analysis. Rotorcraft MAVs represent an excellent alternative due to its versatile flight profile as hovering, vertical take-off/landing (VTOL) and maneuverability, allowing the access to small enclosures or navigate within unstructured environments. Indeed, actual proficiency of navigation and control algorithms has allowed the incursion of VTOL MAVs in other civilian applications as wildlife study, urban surveillance (car and pedestrian traffic), and pollution monitoring, to mention just a few.

However, despite the actual application range of MAVs, the operational role of these air robots remains limited (passive agent) in the mission context, restricting them to surveillance tasks. Enhancing the current profile of civilian MAVs implies the integration of novel operational capabilities to go beyond the aerial medium. For instance, air robots intended to evolve in terrestrial mediums (Multimodal MAVs - MMAVs) require an additional locomotion system. Likewise, those attempting to interact with the surrounding environment (interactive MAVs - iMAVs) need additional actuators (gripper(s), arm(s), tool(s)). These novel applications represent important scientific and technical challenges for different domains involving mechanics, control, artificial vision, embedded systems, etc.

Reduced payload-carrying capacity of multirotor MAVs, as quad-rotors, represents an critical issue while transporting cargo or aerial grasping. However, multiple vehicles are able to overcome this issue, as demonstrated by [5] and [6], where a quad-rotors fleet transport a cargo through grippers or cables, respectively. In [4] presents the planar model, attitude control analysis and outdoors experimental validation of a middle-size helicopter equipped with a compliant gripper capable of robust grasping and transporting objects of different shapes and dimensions. An alternative UAV configuration equipped with a hook intended to deliver/retriving cargo using a vision-based strategy is presented in [7]. In [8], the problem of slung load transportation using autonomous small size helicopters is addressed. The modeling and control of a variable number of helicopters transporting a load is presented. Indeed, the proposed controller prevent and compensate oscillations of load during the flight, which is demonstrated by real flight load transportation by three helicopters.

Merging the 3D mobility of VTOL MAVs with robot manipulators yields an unique blend of capabilities that allows the remote interaction with the surrounding environment. Whereas this concept is very promising, it also comes with significant challenges. Foremost amongst these is the modeling the composite mechanical system and the design of robust controllers against couplings and/or external disturbances that guarantee the stability over partial/complete operational regime. Specifically, this paper deals with an aerial system composed of a quad-rotor MAV having onboard an one-degree-of-freedom (1DOF) manipulator capable of grasping small loads. Our proposal differs from configurations cited above, whose end-effector (gripper) is directly attached to the helicopter's airframe. The actual configuration focuses on reaching targets beyond the quad-rotor's geometry granting access to MAV-denied environments. Likewise, additional DOFs provided by the manipulator attenuates the influence of disturbed/erroneous hovering position (wind-gusts, ground effect) during grasping tasks. On the other hand, the presented configuration

J. Escareno, G. Flores and R. Lozano are with he Heudiasyc Laboratory UMR 7253, Université de Technologie de Compiègne juanantonio.escareno@femto-st.fr, gfloresc@hds.utc, rlozano@hds.utc.fr

M. Rakotondrabe are with the FEMTO-ST Institute, UMR CNRS - UFC / ENSMM / UTBM, Automatic Control and Micro-Mechatronic Deparment, 24, rue Alain Savary, Besancon, France juanantonio.escareno@femto-st.fr, mrakoton@femto-st.fr

restricts the payload capacity of the vehicle, reducing the variety of grasping tasks.

The equations of motion for the composite dynamics of the interactive flying robot are obtained through the Lagrangian formalism, that provides in a natural way the couplings between mechanical subsystems [9][10]. The proposed configuration may be seen as combination of a slung-load-like problem with aerial grasping, which is very attractive from a control perspective. In terms of control, a robust-adaptive control strategy is proposed to achieve the motion control objective of the quad-rotor while the manipulator is driven to desired position carrying a load.

This work is organized as follows: section II describes the problem arising from having a robotic arm onboard of an miniature vehicle, as well as, is derived the rotational mathematical model of the iMAV. Two control strategies are proposed to deal with inherent dynamic couplings, such designs are presented in III. Numerical simulations results are presented in section IV. Conclusions and perspectives are finally given in Section V.

II. Dynamic Model

Consider a quad-rotor MAV evolving within the longitudinal plane, capable to interact with the surrounding environment by means of a 1DOF onboard manipulator. The robotic arm is intended to perform basic prehension (grasping and holding) tasks regarding to placing/recovering objects (sensors, camera, RFID tags, WiFi link, etc.) into/from constrained cavities, as well as transporting tasks. Such grasping/trasporting tasks are performed during near-hovering or in-motion maneuvers.

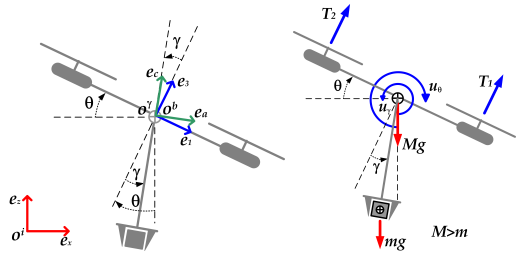

(a) (b)

Fig. 1. Freebody diagram: (a) iMAV reference frames and (b) planar freebody diagram

According to figure (Fig. 1), θ is the pitch angle, γ is the the manipulator's angle with respect to (w.r.t.) $-e_3$, while $T_1$and T_2 are the thrust provided by frontal and rear rotors, respectively. The kinematics of the flying robot comprise two right-handed reference coordinates systems[11].

- Let (e_x, e_y, e_z) defines the fixed inertial coordinates system $\mathcal{F}^i$, whose origin O^i located at the earth surface. For the longitudinal case the vector basis becomes $(e_x, 0, e_z)$
- Let (e_1, e_2, e_3) be the body-fixed frame $\mathcal{F}^b$, whose origin O^b corresponds to the center of gravity CG of the quadrotor. For the longitudinal case the vector basis becomes (e_1, e_3).
- Figure Fig. 1 depicts the vehicle rotating clockwise (righthanded sense) while the manipulator does in the opposite sense. This rotational behavior is expressed by the orthogonal transformation matrix.

$$\mathcal{R}(\theta-\gamma) = \begin{pmatrix} \cos(\theta-\gamma) & \sin(\theta-\gamma) \\ -\sin(\theta-\gamma) & \cos(\theta-\gamma) \end{pmatrix} \quad (1)$$

where θ and γ correspond to the quad-rotor's attitude and manipulator's joint angle, respectively.

1) Kinetic Energy.
The total kinetic energy function $\mathcal{K}(\dot\theta, \dot\gamma)$ of the multi-body mechanic system resulting from the rotational and translational motion can be partitioned by the sum of the the quad-rotor's kinetic energy,

$$\mathcal{K}_M(\dot\theta) = \frac{1}{2} I_Y \dot\theta^2 + \frac{1}{2} M\dot x^2 + \frac{1}{2} M \dot z^2 \quad (2)$$

and the manipulator's kinetic energy

$$\mathcal{K}_m(\dot\gamma, \dot\theta) = \frac{1}{2} I_y (\dot\theta - \dot\gamma)^2 + \frac{1}{2} m \dot x_m^2 + \frac{1}{2} m \dot z_m^2 \quad (3)$$

where

$$\begin{aligned} x_m &= x - \ell \sin(\theta-\gamma) \\ z_m &= z - \ell \cos(\theta-\gamma) \end{aligned}$$

are the coordinate of the manipulator center of gravity CG_m, ℓ is the distance from the pivot to the manipulator's CG_m, $\dot\theta$ denotes the angular velocity of the body frame, I_Y and I_y are the inertia mass-moment of the quad-rotor airframe and manipulator, while M and m represents the mass of the quad-rotor and the manipulator, respectively.

2) Potential Energy Likewise, the potential energy of the $iMAV$ is given by the sum of quad-rotor's and manipulator's potential energies [10]

$$P = Mgz + mg\left[z - \ell\left(1 - \cos(\theta-\gamma)\right)\right] \quad (4)$$

Using (2), (3) and (4) given above, the Lagrangian may be written as

$$\begin{aligned} \mathcal{L} = \; & \tfrac{1}{2}(M+m)\dot x^2 + \tfrac{1}{2}(M+m)\dot z^2 + \tfrac{1}{2} I_Y \dot\theta^2 \\ & + \tfrac{1}{2}(m\ell^2 + I_y)(\dot\theta - \dot\gamma)^2 - m\ell\cos(\theta-\gamma)\dot x(\dot\theta - \dot\gamma) \\ & + m\ell\sin(\theta-\gamma)\dot z(\dot\theta - \dot\gamma) - Mgz \\ & - mg\left[z - \ell\left(1-\cos(\theta-\gamma)\right)\right] \end{aligned} \quad (5)$$

A. Equations of motion

Applying the Euler-Lagrange formulation we obtain the equations modeling the overall motion of the iMAV, i.e. the translational

$$\begin{cases} u_x = & (M+m)\ddot x - m\ell\cos(\theta-\gamma)(\ddot\theta - \ddot\gamma) \\ & + m\ell\sin(\theta-\gamma)(\dot\theta - \dot\gamma)^2 \\ u_z = & (M+m)\ddot z + m\ell\sin(\theta-\gamma)(\ddot\theta - \ddot\gamma) \\ & + m\ell\cos(\theta-\gamma)(\dot\theta - \dot\gamma)^2 + (M+m)g \end{cases} \quad (6)$$

notice that for the translational equation, displacement along the $x-$axis is underactuated by the attitude, i.e. $u_x = 0$. The corresponding equations describing the rotational motion are

$$\begin{cases} u_\theta = & (I_Y + I_y + m\ell^2)\ddot{\theta} - (m\ell^2 + I_y)\ddot{\gamma} - m\ell\cos(\theta-\gamma)\ddot{x} \\ & +m\ell\sin(\theta-\gamma)\ddot{z} + mg\ell\sin(\theta-\gamma) \\ u_\gamma = & (I_y + m\ell^2)\ddot{\gamma} - (ml^2 + I_y)\ddot{\theta} + m\ell\cos(\theta-\gamma)\ddot{x} \\ & -m\ell\sin(\theta-\gamma)\ddot{z} - mg\ell\sin(\theta-\gamma) \end{cases} \tag{7}$$

The set of scalar motion equations, translational (6) and rotational (7), obtained from the Lagrange formulation are grouped in compact vectorial expressions.

1) Translational Motion:

$$(M+m)\dot{\mathcal{V}} = \mathcal{U}_\xi + \mathcal{W}_{(M+m)} + \mathcal{F}_c \tag{8}$$

where $\mathcal{V} = (\dot{x}, \dot{z})^T$ represents the 2D velocity of the drone, $\mathcal{U}_\xi = (0, u_z)^T$ denotes the thrust vector used as control input, $\mathcal{W}_{(M+m)} = (0, -(M+m)g)^T$ is the total weight vector and $\mathcal{F}_c$ is the coupling force vector provided by manipulation subsystem, which is written as

$$\mathcal{F}_c = \begin{pmatrix} m\ell\cos(\theta-\gamma)(\ddot{\theta}-\ddot{\gamma}) - m\ell\sin(\theta-\gamma)(\dot{\theta}-\dot{\gamma})^2 \\ -m\ell\sin(\theta-\gamma)(\ddot{\theta}-\ddot{\gamma}) - m\ell\cos(\theta-\gamma)(\dot{\theta}-\dot{\gamma})^2 \end{pmatrix} \tag{9}$$

Such term, describes the centrifugal provided by the manipulation subsystem and tangential forces exerted in the drone.

2) Rotational Motion:

$$\mathcal{M}\ddot{\eta} = \mathcal{U}_\eta + \mathcal{G}_\eta + \mathcal{T}_c \tag{10}$$

$\eta = (\theta, \gamma)^T$ stands for the generalized coordinates vector, and $\mathcal{M}$ (symmetric and invertible) represents the inertia matrix

$$\mathcal{M} = \begin{pmatrix} I_Y + I_y + ml^2 & -ml^2 + I_y \\ -ml^2 + I_y & I_y + ml^2 \end{pmatrix} \tag{11}$$

The effects of the mass are visible in vector $\mathcal{G}$

$$\mathcal{G}_\eta = \begin{pmatrix} -mgl\sin(\theta-\gamma) \\ mgl\sin(\theta-\gamma) \end{pmatrix} \tag{12}$$

as well as couplings are depicted by $\mathcal{T}_c$, written as

$$\mathcal{T}_c = \begin{pmatrix} ml\cos(\theta-\gamma)\ddot{x} - ml\sin(\theta-\gamma)\ddot{z} \\ -ml\cos(\theta-\gamma)\ddot{x} + ml\sin(\theta-\gamma)\ddot{z} \end{pmatrix} \tag{13}$$

III. Control Strategy

In this section we present the control strategy, which is based on a hierarchical scheme considering the well-known time-scale separation between rotational and translational dynamics. The main goal is to drive the rotorcraft drone according to the commanded reference while rejecting coupling disturbances provided by the evolution of the onboard manipulator. The use of a hierarchical approach allows to synthesize modular control algorithms for the inner- and outer-loop dynamics, respectively. Since the quadrotor features an underactuated dynamic nature, i.e. translation relays on rotational motion. Thus, the control design must provide robust stability to the inner-loop (rotational subsystem) to guarantee the effectiveness of the outer-loop control (translational motion).

A. Standard H_∞ robust control of the inner-loop

We present in this subsection the calculation of the controller $C_\eta(s)$ of the internal loop in order to enhance the performances the rotation. For that, we propose to use standard H_∞ approach because of its robustness relative to the uncertainties and also relative to external disturbances. Indeed, it is possible to account *a priori* these disturbances during the calculation of the controller such that performances will still be maintained in their presence (performances robustness). In our case, the disturbance is given by $\mathcal{G}_\eta + \mathcal{T}_c$.

1) Modeling: From the rotation model in the time domain as in (10), we derive the rotation model in the Laplace domain:

$$\eta = G_\eta(s)\left(\mathcal{U}_\eta + \mathcal{D}_\eta\right) \tag{14}$$

where $\mathcal{D}_\eta = \mathcal{G}_\eta + \mathcal{T}_c$ is an input disturbance and

$$G_\eta(s) = \begin{pmatrix} \frac{g_{11}}{s^2} & \frac{g_{12}}{s^2} \\ \frac{g_{21}}{s^2} & \frac{g_{22}}{s^2} \end{pmatrix} = \frac{1}{s^2}\mathcal{M}^{-1} \tag{15}$$

such that $g_{ij} \in \mathbb{R}$.

Fig. 2 pictures the block diagram of the internal closed-loop including the system $G_\eta(s)$ and the controller $C_\eta(s)$ to be synthesized. In the figure, η_d indicates the desired angle. The following specifications will be used for the calculation of the controller.

Tracking performances specifications - For each angles in η, we impose the following requirements:

- a settling time no more than $300ms$,
- a maximal overshoot of 10%,
- a statical error less than 1%.

Disturbance rejection - The characterization shown that the disturbance $\mathcal{G}_\eta$ has a maximal amplitude of $\mathcal{G}_\eta^{max} = 0.145$ while the disturbance $\mathcal{T}_c$ has an infinite norm of $\|\mathcal{T}_c\|_\infty = 0.1$. Consequently, it is specified that the corresponding maximal disturbance $\mathcal{D}_\eta$ will imply a maximal angle error of 3^o, that is: $\frac{3^o}{(0.145+0.1)}$ is the maximal error due to disturbance.

Command moderation - With only the above two specifications, it is difficult to compute a convenient H_∞ controller. Indeed, the calculated controller led to unstability when simulated due to numerical limitation such as the minimal sampling time possible. This numerical problem can be solved by introducing a shaping to the command signal and that will moderate (limit) it. Different tests show that a maximal ratio of $\frac{\mathcal{U}_\eta}{\eta_d} = \frac{1.95}{45^o}$ is a convenient for each of the two axis of η.

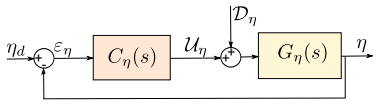

Fig. 2. Closed-loop scheme of the internal loop.

2) Standard form and standard H_∞ problem: From the above specifications, three weighting functions denoted $\mathcal{W}_1$, $\mathcal{W}_2$ and $\mathcal{W}_3$ are systematically introduced: the first one to weight the error signal ε_η in order to account the tracking performances, the second one to weight the input disturbance signal $\mathcal{D}_\eta$ in order to account its rejection specifications and the last one to weight the command signal $\mathcal{U}_\eta$. Fig. 4-a pictures the corresponding weighted closed-loop in which o_ε is the weighted output error signal, o_u is the weighted command signal and i_η is the new disturbance accounting the weighting function. From this scheme, the standard scheme used for the controller synthesis is derived (Fig. 4-b). It consists of the interconnection between an augmented system $\mathcal{P}_\eta(s)$ and the controller to be synthesized. The input of the interconnection are composed of the exogenous signals η_d and i_η while the output is composed of the weighted signals o_ε and o_u.

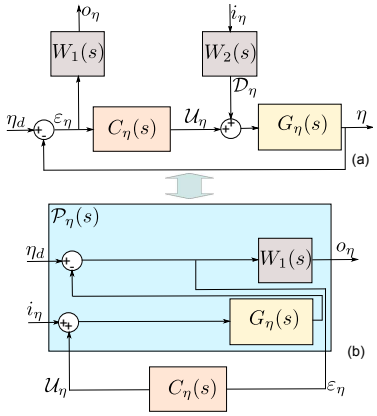

Fig. 3. (a): weighted closed-loop scheme. (b): the standard scheme.

The standard H_∞ problem consists in finding an optimal value $\gamma > 0$ and the controller $C_\eta(s)$ stabilizing the interconnection in Fig. 4-b and guaranteeing the following inequality [14]:

$$\left\|\mathcal{F}_l\left(\mathcal{P}_\eta(s), C_\eta(s)\right)\right\|_\infty < \gamma \tag{16}$$

where $\mathcal{F}_l\left(\mathcal{P}_\eta(s), C_\eta(s)\right)$ is the lower linear fractionnar transformation between $\mathcal{P}_\eta(s)$ and$C_\eta(s)$ defined here as follows:

$$\begin{pmatrix} o_\varepsilon \\ o_u \end{pmatrix} = \mathcal{F}_l\left(\mathcal{P}_\eta(s), C_\eta(s)\right) \begin{pmatrix} \eta_d \\ i_\eta \end{pmatrix} \tag{17}$$

From Fig. 4-a, we have:

$$\begin{cases} o_\varepsilon = W_1 S_\eta \eta_d - W_1 G_\eta S_\eta W_2 i_\eta \\ o_u = W_3 C_\eta S_\eta \eta_d - W_3 C_\eta G_\eta S_\eta W_2 i_\eta \end{cases} \tag{18}$$

where $S_\eta = (I + G_\eta C_\eta)^{-1}$ is the sensivity function.

Using (Inequa. 16) and (Equ. 18), the standard H_∞ problem becomes into finding $C_\eta(s)$ and an optimal value of γ such that:

$$\begin{cases} \|W_1 S_\eta\|_\infty < \gamma \\ \|-W_1 G_\eta S_\eta W_2\|_\infty < \gamma \\ \|W_3 C_\eta S_\eta\|_\infty < \gamma \\ \|-W_3 C_\eta G_\eta S_\eta W_2\|_\infty < \gamma \end{cases} \tag{19}$$

which is satisfied if we find a controller ensuring the following inequalities:

$$\begin{cases} |S_\eta| = \bar{\sigma}_{S_\eta} < \gamma \left|\frac{1}{W_1}\right| \\ |G_\eta S_\eta| = \bar{\sigma}_{G_\eta S_\eta} < \gamma \left|\frac{1}{W_1 W_2}\right| \\ |C_\eta S_\eta| = \bar{\sigma}_{C_\eta S_\eta} < \gamma \left|\frac{1}{W_3}\right| \\ |C_\eta G_\eta S_\eta| = \bar{\sigma}_{C_\eta G_\eta S_\eta} < \gamma \left|\frac{1}{W_3 W_2}\right| \end{cases} \tag{20}$$

where $\bar{\sigma}_{S_\eta}$, $\bar{\sigma}_{G_\eta S_\eta}$, $\bar{\sigma}_{C_\eta S_\eta}$ and $\bar{\sigma}_{C_\eta G_\eta S_\eta}$ are the upper singular values of S_η, of $G_\eta S_\eta$, of $C_\eta S_\eta$ and of $C_\eta G_\eta S_\eta$ respectively. The problem in (Equ. 20) is called a 4-blocks mixed sensivity. To solve this problem, we use the Glover-Doyle algorithm [15]. The transfers $\frac{1}{W_1(s)}$ and $\frac{1}{W_1 W_2}$ are called gabarits or bounds and are calculated from the specifications in Section. III-A.1 as we will present in the next subsection.

3) Derivation of the weighting functions: To obtain the gabarit $\frac{1}{W_1(s)}$, the specifications of tracking performances are used. To account the statical error, the settling time and the no-overshoot transient part, we propose the following gabarit:

$$\frac{1}{W_1} = \frac{0.1003s + 0.01}{0.04778s + 1} \tag{21}$$

Concerning the gabarit $\frac{1}{W_1 W_2}$, the disturbances rejection specifications are used. As a rejection of $\frac{\varepsilon_\eta}{\mathcal{D}_\eta} = 2\%$ is wanted for any frequency, we choose:

$$\frac{1}{W_1 W_2} = \frac{3^o}{(0.145 + 0.1)} \tag{22}$$

The weightings W_1 and W_2 can be afterwards derived from (Equ. 21) and (Equ. 22).

Finally, the gabarit $\frac{1}{W_3(s)}$ is derived from the specifications concerning the command moderation. We use:

$$\frac{1}{W_3(s)} = \frac{1.95}{45} \tag{23}$$

4) Calculation of the controller: The controller (a matrix transfer function with four elements) has been calculated. We find find a matrix where each element has an order of 8. The optimal value of γ is: $\gamma_{optimal} = 3.63$. From these curves, we remark that the controller will not necessarily satisfy the specifications (as predicited by the $\gamma_{optimal}$ which is superior to one) mainly for the distrubance rejection and for the command moderation. However, as we can remark, the tracking performances will be satisfied. Concerning the distrubance rejection, the non-satisfaction will be at very low frequency. However, this case of disturbance will rarely happen during the functioning of the rotorcraft. On the other hand, the command moderation is not satisfied at high frequency (for one angle). Although this, the general performances of the rotorcraft are still in accordance with the initial expectation (tracking performances and disturbance rejection).

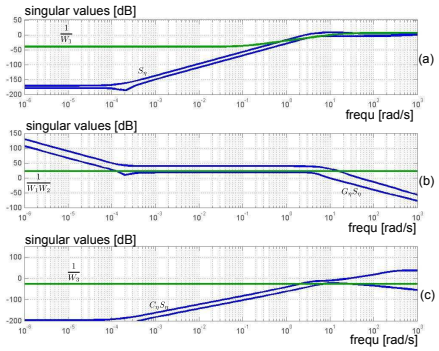

Fig. 4. (a): singular values of S_η and of the gabarit $\frac{1}{W_1}$. (b): singular values of $G_\eta S_\eta$ and of the gabarit $\frac{1}{W_1 W_2}$. (c): singular values of $C_\eta S_\eta$ and of the gabarit $\frac{1}{W_3}$.

B. Outer-loop Control

In order to apply the SMC[13] scheme to system described by (Fig. 8),as first step we define the corresponding sliding surface vector $\mathcal{S} = (s_x, s_z)^T$ as

$$\mathcal{S} = \dot{\tilde{\xi}} + \Lambda \tilde{\xi} \tag{24}$$

where $\Lambda = \text{diag}(\lambda_x, \lambda_z)$ is a definite-positive tunable matrix and $\tilde{\xi} = \xi - \xi^d$ stands for the position error vector. The problem of tracking the desired vector $\xi^d = (x^d, z^d)^T$ is equivalent to stabilize the first-order dynamics $\dot{\mathcal{S}}$

$$\dot{\mathcal{S}} = \frac{1}{M+m}\left[\mathcal{U}_\xi + \mathcal{W}_{(M+m)} + \mathcal{F}_c\right] - \ddot{\xi}^d + \Lambda \dot{\tilde{\xi}} \tag{25}$$

where $\mathcal{F}_c$ verifies $\|\mathcal{F}_c\| \leq \beta$. The system (25) is stabilized using the controller

$$\mathcal{U}_\xi = (M+m)\left(-K_p \mathcal{S} - K_\alpha \text{sign}(\mathcal{S}) - \Lambda \dot{\tilde{\xi}}_x + \ddot{\xi}^d + g e_z\right) \tag{26}$$

where $K_p = \text{diag}(k_{p_x}, k_{p_z})$ and $K_\alpha = \text{diag}(\alpha_x, \alpha_z)$ are definite-positive matrices.

Parameter	Value[units]
l	0.35[m]
M	0.4[Kg]
m	0.03 [Kg]
I_Y	0.177 [Kgm^2]
I_y	3.0625×10^{-4}
g	9.8×10^{-4} [Kgm^2]

TABLE I
INTERACTIVE ROTORCRAFT VEHICLE

1) Stability proof: In order to provide a controller that guarantees the convergence of state vector to the equilibrium, consider the following candidate Lyapunov function (CLF)

$$\mathcal{V} = \frac{1}{2}\mathcal{S}^T\mathcal{S} \tag{27}$$

Differentiating with respect to time Equ. 8, and using Equ. 26

$$\dot{V} = \mathcal{S}^T\left(-K_p\mathcal{S} - K_\alpha \text{sign}(\mathcal{S}) + \frac{\mathcal{F}_c}{M+m}\right) \tag{28}$$

$$\dot{V} \leq -\lambda_m\{K_p\}\|\mathcal{S}\|^2 - \lambda_m\{K_\alpha\}\|\mathcal{S}\|\|\text{sign}(\mathcal{S})\| + \frac{\|\mathcal{S}\|\|\mathcal{F}_c\|}{M+m} \tag{29}$$

where $\lambda_m\{\cdot\}$ represent a matrix's minimal eigenvalue. Now, using the following properties:

- $\|\mathbf{x}\|\|\mathbf{y}\| \geq |\mathbf{x}^T\mathbf{y}|$
- $\|\mathbf{x}\| \leq \|\mathbf{x}\|_1$

we get

$$\dot{V} \leq -\lambda_m\{K_p\}\|\mathcal{S}\|^2 - \|\mathcal{S}\|_1\left(\frac{\|\mathcal{F}_c\|}{M+m} - \lambda_m\{K_\alpha\}\right) \tag{30}$$

where it is know that $\|\mathcal{F}_c\| \leq \beta$, then we obtain

$$\dot{V} \leq -\lambda_m\{K_p\}\|\mathcal{S}\|^2 - \|\mathcal{S}\|_1\left(\frac{\beta}{M+m} - \lambda_m\{K_\alpha\}\right) \tag{31}$$

Hence, to assure the negativity of the CLF, we assign

$$\lambda_m\{K_\alpha\} = \frac{\beta}{M+m} + \nu \tag{32}$$

with $\nu > 0$, which results in

$$\dot{V} < -\lambda_m\{K_p\}\|\mathcal{S}\|^2 - \nu\|\mathcal{S}\|_1 \tag{33}$$

The latter implies that the trajectory of $\mathcal{S}$ converges to the origin, which means that the trajectory-tracking objective is fulfilled.

IV. Numerical Simulation

Numerical simulations were carried out in order to support the proposed control algorithms evaluating the performance of the rotational and translational disturbed subsystems. In the simulation we use the parameters close to real aerial platforms. Such parameters are depicted on table I

In Fig. 5 is depicted the evolution of the states during the translation task consisting in reaching $\xi^d = (x^d = 2, z^d = 4)^T$, while the arm is meant to reach an desired

angle of $\gamma_d = 35\,\text{deg}$. It is shown that the rotational subsystem fulfil the performance control requirements. Likewise, the translational subsystem is able to cope with the disturbance introduced by the motion of the rotational subsystem, particulary the manipilator.

Concerning the control inputs , in figure figure Fig. 6 we observe that the magnitude of control inputs remains within actual limited response (saturation). The control of the translational

V. Concluding remarks and perspectives

The present paper addressed the modeling and control of a rotorcraft configuration that features an onboard robotic manipulator. The modeling, obtained via the Euler-Lagrange formalism, was meant to identify the intrinsic relationships resulting from this kind of multi-body (helicopter-manipulator) air vehicle. Based on the equations of motion provided by the model, we utilise a hierarchical scheme as overall control strategy. For the controller synthesis, a classical time-scale separation is considered between rotational (fast-dynamics inner-loop) and translational motion (slow-dynamics outer loop). Considering that couplings are considered as disturbances in the present study, we use a SMC approach to deal with the stabilization of the outer-loop, while inner-loop is tackled via a H_∞-based controller. Since the inner-loop represents the core of control strategy, the use of the H_∞ technique obeys to the fact that, such approach allows to set specific performance features (response time, static error amount, etc) by means of weighting functions. The implementation of such controllers leads to a satisfactorily evolution of the system states fulfilling the control objective.

References

[1] R. Bachmann, F. Boria, P. Ifju, R. Quinn, J. E. Kline, R. Vaidyanathan, "Utility of Sensor Platform Capable of Aerial and Terrestrial Locomotion". *International Conference on Advanced Intelligent Mechatronics*. Monterey, California, USA, 24-28 July, 2005.

[2] , R. Cory and R. Tedrake, "Experiments in Fixed-Wing UAV Perching", *26th AIAA Applied Aerodynamics Conference*, 18 - 21 Aug 2008 Hawaii Convention Center.

[3] Mark R. Cutkosky, Alan T. Abeck and Alexis Lussier Desbiens, "Landing, perching and taking off from vertical surfaces". *Journal International Journal of Robotics Research archive*, Volume 30 Issue 3, March 2011

[4] Paul E. Pound, Daniel R. Bersak and Aaron M. Dollar, Grasping From the Air: Hovering Capture and Load Stability, *IEEE International Conference on Robotics and Automation*, Shanghai, China, May. 2011.

[5] Mellinger, N. Michael, and V. Kumar. Trajectory generation and control for precise aggressive maneuvers with quadrotors. In Int. Symposium on Experimental Robotics, New Delhi, India, Dec. 2010.

[6] D. Mellinger, M. Shomin, and V. Kumar. Control of quadrotors for robust perching and landing. In Proceedings of the International Powered Lift Conference, Oct 2010.

[7] N. Kuntz, P. Y. Oh, Towards Autonomous Cargo Deployment and Retrieval by an Unmanned Aerial Vehicle Using Visual Servoing,, in *2008 ASME Dynamic Systems and Controls Conference*.

[8] M. Bernard, K. Kondak and G. Hommel, Load Transportation System based on Autonomous Small Size Helicopters, *The aeronautical Joutnal*, March 2010 Vol. 114 No. 1153.

[9] Goldstein, H.: Classical Mechanics. Addison-Wesley. ISBN 0201029693 (1980)

[10] Fantoni,I. and Lozano,R.(2002). Nonlinear control for underactuated mechanical systems. In Communications and control engineering series, 2002, Springer.

[11] Etkin, B., Reid, L.D.: Dynamics of Flight. Wiley, New York. ISBN 0471034185 (1959)

[12] S. Salazar, J. Escareno, D. Lara and R. Lozano, Embedded control system for a four rotor UAV, *International Journal of Adaptive Control and Signal Processing*, vol. 21, issue 2-3, pp. 189-204, March-April 2007.

[13] Slotine and Weiping Li. Applied nonlinear control, Prentice-Hall, Englewood Cliffs, NJ (1991)

[14] G. J. Balas, J. C. Doyle, K. Glover, A. Packard and R. Smith, "μ-analysis and synthesis toolbox", The Mathworks User's Guide-3, 2001.

[15] J. C. Doyle, K. Glover, P. K. Khargonekar and B. A. Francis, "State-space solutions to standard H_2 and H_∞ control problems", IEEE Transactions on Automatic Control, AC 34 No.8, pp.831-846, 1989.

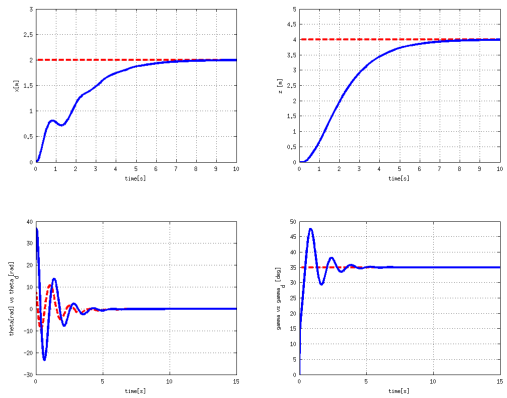

Fig. 5. States evolution: [Top:] Translational states,[Bottom:] Rotational states

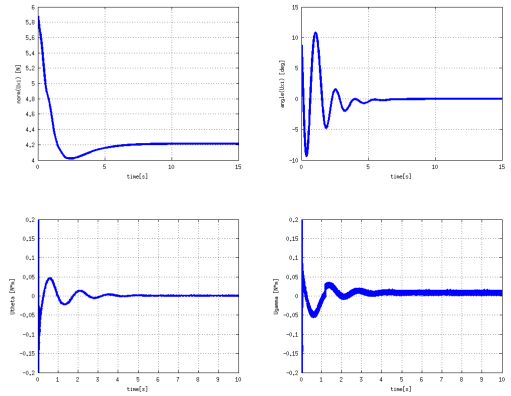

Fig. 6. Control Inputs: displacement evolution of the piezocantilever